

# THE GLOBULAR CLUSTER SYSTEMS IN THE COMA ELLIPTICALS. I: THE LUMINOSITY FUNCTION IN NGC 4874, AND IMPLICATIONS FOR HUBBLE’S CONSTANT<sup>1</sup>

J. J. KAVELAARS AND WILLIAM E. HARRIS

Department of Physics and Astronomy, McMaster University, Hamilton ON L8S 4M1, CANADA; kavelaar,harris@physics.mcmaster.ca

DAVID A. HANES

Department of Physics, Queen’s University, Kingston ON K7L 3N6, CANADA; hanes@astro.queensu.ca

JAMES E. HESSER

Dominion Astrophysical Observatory, Herzberg Institute of Astrophysics, National Research Council, 5071 West Saanich Road, Victoria BC V8W 3P6, CANADA; jim.hesser@hia.nrc.ca

AND

CHRISTOPHER J. PRITCHET

Department of Physics and Astronomy, University of Victoria, Box 3055, Victoria, BC V8W 3P6, CANADA; pritchet@phys.uvic.ca

*accepted for publication in the Astrophysical Journal*

## ABSTRACT

We have used deep HST/WFPC2 images in  $V$  (F606W) and  $I$  (F814W) to measure the luminosity distribution of the globular clusters in NGC 4874, the central cD galaxy of the Coma cluster. We find the “turnover” point of the globular cluster luminosity function (GCLF) to lie at  $V = 27.88 \pm 0.12$ , while the overall GCLF shape matches the standard Gaussian-like form with dispersion  $\sigma_V = 1.49 \pm 0.12$ . We use the GCLF as a standard candle by matching the turnover points in NGC 4874 and another Coma elliptical, IC 4051, with those of the giant ellipticals in the Virgo cluster (M87 and five others). The result is  $\Delta(m - M)(\text{Coma} - \text{Virgo}) = 4.06 \pm 0.11$  magnitudes, which converts to a Coma distance  $d = 102$  Mpc if the Virgo distance modulus is  $(m - M)_0 = 30.99 \pm 0.04$ . The Hubble constant which emerges from our GCLF measurement is then  $H_0 = (69 \pm 9) \text{ km s}^{-1} \text{ Mpc}^{-1}$ . We confirm this  $H_0$  value with a novel presentation of the “Hubble diagram” for GCLFs in giant E galaxies. Measurements of additional GCLFs in the Coma ellipticals, as well as calibrating galaxies in Virgo and Fornax, have excellent potential to refine this result in the near future.

*Subject headings:* Cosmology: Distance Scale – Galaxies: Individual – Galaxies: Star Clusters

## 1. INTRODUCTION

One of the simplest and longest-range stellar standard candles for distance measurement is the globular cluster luminosity function (GCLF). The number distribution of globular clusters per unit magnitude has long been known to have a unimodal and roughly symmetric form, with a peak frequency or “turnover” in the range  $M_V^0 \sim -7.4 \pm 0.2$  in both spiral and elliptical galaxies. Theoretical concerns have often been expressed that the mass distribution of globular clusters (and thus the GCLF) might be expected to depend on external factors such as galaxy type, metallicity, or radial location within a galaxy; but the empirical evidence strongly suggests that these factors exert remarkably little influence on the peak of the GCLF (see Jacoby et al. 1992; Whitmore 1996; Ashman et al. 1995; Harris 1999 for thorough discussions). With the imaging capabilities of the Hub-

ble Space Telescope, the GCLF turnover is within reach for any galaxy up to at least 120 Mpc, beyond the regime of local peculiar motions which might strongly bias measurements of the Hubble constant  $H_0$ .

For purposes of remote distance calibration and estimation of  $H_0$ , the globular cluster populations in giant elliptical galaxies are by far the most interesting targets, simply because of the sheer size of their cluster populations and thus the ability to define the GCLF shape and turnover with high statistical confidence. It is also a fortunate coincidence for this distance-scale method that the very most populous globular cluster systems inhabit the supergiant ellipticals that lie at the centers of rich clusters of galaxies, which are the very objects that are the main landmarks in the Hubble flow.

In this paper we present our new measurement of

<sup>1</sup>Based on observations obtained with the NASA/ESA *Hubble Space Telescope*, obtained at the Space Telescope Science Institute, which is operated by the Association of Universities for Research in Astronomy, Inc., under NASA contract NAS 5-26555.

the GCLF turnover for the globular cluster system in NGC 4874, the central cD elliptical in the Coma cluster, and use it to estimate  $H_0$ . The bright end of the GCLF in NGC 4874 has already been studied with ground-based imaging, which indicated that it indeed has a large globular cluster system (Harris 1987; Thompson & Valdes 1987; Blakeslee & Tonry 1995). With the much deeper HST photometric limits, we could therefore confidently expect to garner a huge population of clusters to define the GCLF.

## 2. THE DATA

Our raw dataset consists of 18  $V$  (F606W) and 10  $I$  (F814W) images of various exposure lengths (see Table 1), taken 1997 August 16 and 24 (program GO-5905) with the WFPC2 camera. The long exposures were sub-pixel-shifted (dithered) in a pentagonal pattern by fractional pixel amounts in order to reconstruct clean composite images free from cosmic-ray contamination and bad-pixel artifacts. The  $V$  exposures, totaling 20940 sec, were taken to probe the GCLF deeply enough to resolve the turnover point, while the  $I$  exposures, totaling 8720 sec, were used to define the color (metallicity) distribution for the brighter end of the cluster system. The color distribution, spatial structure of the GCS, and the specific frequency will be discussed in Paper II (Harris et al. 1999). Here, we analyze the GCLF and use it to estimate the distance to Coma and thus  $H_0$ .

To maximize the total globular cluster population falling within the WFPC2 field of view, we placed the center of the PC1 CCD on the nucleus of NGC 4874. A few other large elliptical galaxies projected near the center of Coma fall on the outskirts of the WF2,3,4 CCDs; however, these proved not to have significant numbers of globular clusters of their own and thus did not contaminate the NGC 4874 sample. Small areas surrounding them were, in any case, masked out in all subsequent data analysis.

We first retrieved the raw data from the HST archive located at the CADC<sup>2</sup>. The CADC pipeline preprocessed the images at this point, with the best calibration images then available. We then combined the exposures in pairs (the pairs of long exposures within each orbit) to define a first set of frames reasonably free of cosmic-ray contamination.

The vast majority of detected objects on the frames are the globular clusters in the halo of NGC 4874. At the  $\sim 100$ –Mpc distance of Coma they appear as unresolved point sources even in the PC1 frames, so it is readily possible to perform conventional point-spread function (PSF) photometry on the frames.

We constructed an independent PSF for each image and each of the four WFPC2 CCDs. With DAOPHOT and ALLSTAR (Stetson 1994) we then generated separate lists of candidate starlike (that is, unresolved) objects on each frame. These coordinate lists were used to determine the (small) offsets and rotations to map the images onto a common re-registered coordinate system. Next, Stetson’s (1994) MONTAGE2 code was used to define a “master” image in each filter as the median (i.e., 50th percentile) of the individual exposures. Finally, we summed the master  $V$  and  $I$  images to generate a single deep, contamination-free image which maximized the available flux for object detection.

The photometry must also be designed to avoid false detections and nonstellar objects (noise spikes, small, faint background galaxies, or even compact dwarf galaxies within Coma itself). The real and artificial-star measurements were therefore combined with image shape parameters (the DAOPHOT parameters SHARP and  $\chi$ , and the radial image moment  $r_1$  defined by Kron 1980 and Harris et al. 1991). Several numerical trials were carried out with the artificial-star data to vary the detection threshold (in units of  $\sigma_s$ , the RMS scatter of the sky background) and the shape selection parameters, and thus to determine the highest values of these thresholds which would not deteriorate the detection efficiency of genuine starlike objects (see Figure 1). We adopted a DAOPHOT/FIND detection threshold of  $3.5\sigma_s$  above sky (c.f. Stetson 1987), a level which recovered virtually all the brighter input artificial stars while adding almost no false detections from noise. The adopted boundaries for  $\chi$ , SHARP, and  $r_1$  resulted in the culling of about 5% of the artificial stars, mostly at the faintest levels where the distinction between starlike and nonstellar objects by image shape classification also becomes difficult. At the faint end as well, some unwanted nonstellar objects end up being scattered into the “starlike” category, but these must be statistically removed from the final GCLF by subtraction of the background luminosity function (see below).

With the master list of starlike objects now determined, we used the ALLFRAME code (Stetson 1994) to measure these objects on the original set of F606W and F814W images, employing the individual PSFs for each frame as determined previously. To transform the averaged instrumental magnitudes to the standard  $VI_{KC}$  system we employed the normal transformation equations in Holtzman et al. (1995). For the faint objects lacking any  $I$ –band measurement, we assumed a  $(V - I)$  colour of 0.95, the ob-

<sup>2</sup>Canadian Astronomy Data Centre, operated by the Herzberg Institute of Astrophysics, National Research Council of Canada.

TABLE 1  
*HST* OBSERVING LOG FOR GO 5905

R.A. (J2000)	Decl. (J2000)	Filter	Exposure Times (s)
12 59 33.43	+27 57 43.3	F606W	$3 \times 180$
			$2 \times 1100$
			$14 \times 1300$
		F814W	$4 \times 230$
			$6 \times 1300$

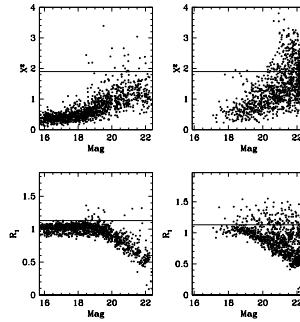


FIG. 1.— Image moments  $\chi$  and  $r_1$  plotted against magnitude. The two panels on the left show artificial-star sequences, while the two on the right show the real objects measured on the WFPC2 frames. Filled circles are objects assumed to be “starlike”, while the open circles are “nonstellar” and culled from the sample.

served mean color of the brighter clusters (see below). The basic transformation used was

$$\begin{aligned} V &= m(F606W) + 0.254(V-I) \\ &\quad + 0.012(V-I)^2 + 22.098 \\ I &= m(F814W) - 0.062(V-I) \\ &\quad + 0.025(V-I)^2 + 20.839, \end{aligned}$$

to which we then added the individual zero-point terms for each chip as listed in Table 2.

In these equations, we have added the standard value of 0.05 mag to the published zero-points to account for the deferred charge transfer effect that produces an offset between long and short exposures (e.g., Stetson et al. (1999)). As a direct check on this offset, we intercompared the magnitudes of several of the brightest stars on our long and short exposures, and found

$$(m_{1300s} - m_{180s})_{F606W} = -0.06 \pm 0.02,$$

$$(m_{1300s} - m_{230s})_{F814W} = -0.06 \pm 0.03.$$

That is to say, magnitudes determined using short exposures (like those used for the calibration of Holtzman et al. 1995) tend to be fainter than those determined using long exposures; our internal tests confirm the  $\simeq 0.05$ -mag offset normally used.

### 3. THE GCLF

Our final catalog of objects with deep  $V$ -band measurements is still contaminated to some extent by a few foreground stars (nearly negligible) and by faint, extremely small galaxies that might have crept through the image classification procedure described above. To define a “background” population, we simply use those objects which lie on the radial outskirts of our field, more than 75 arcseconds (corresponding roughly to 40 kpc) from the center of NGC 4874. At these large radii, we find that the number density of globular clusters is still declining; that is, the total extent of the GCS evidently spills well beyond the borders of our single WFPC2 field. However, the object density within the background area is only a small fraction (14%) of the density in the core region (the area covered by the PC1 chip), so we can use the outer corners for background knowing that it will produce only a small over-subtraction of the globular cluster population itself.

This raw GCLF must be corrected for detection incompleteness at the faint end. The detection probability is, in turn, dependent on the local level of background light and thus is a function of the distance from the galaxy center. Figure 2 shows the

completeness fraction for four radial zones ( $3'' \leq r < 13''$ ,  $13'' \leq r < 22''$ ,  $22'' \leq r < 50''$ ,  $50'' \leq r < 100''$ ). Clearly, the inner zones – mostly within PC1 and within the bright galaxy envelope – have noticeably brighter, but consistent, completeness cutoff levels than in the outer annuli. This radial dependence was explicitly folded in to the completeness corrections to the raw data.

The full completeness-corrected and background-subtracted luminosity functions are shown in Figure 3 and Table 3. The limit of our deep  $V$  photometry reaches the turnover point (GCLF peak) or just past it.

The standard candle of the GCLF method is the luminosity level of the turnover or peak point, which we call  $V^0$ . The immediate goal for this discussion is therefore to estimate this point as accurately as possible given that we see only the bright half of the GCLF and the turnover region itself, and not the faint half. Conventionally, simple interpolation functions such as a Gaussian (e.g., Jacoby et al. 1992) or  $t_5$  (Secker & Harris 1993), both of which have two free parameters ( $V^0$  and the dispersion width), have been used for this purpose since they have repeatedly been shown to match the region near the turnover quite accurately.

For cases such as ours where the photometric limit  $V(\text{lim})$  is fairly close to  $V^0$ , it is important to note that attempts to solve *simultaneously* for both the peak  $V^0$  and dispersion  $\sigma_V$  of the interpolation function are problematic, because the two parameters are correlated (see Secker & Harris 1993; Hanes & Whittaker 1987) and tend to produce overestimates of both the turnover and dispersion when the fit is constrained by only one side of the GCLF. A systematically more accurate procedure is to *adopt* a value for  $\sigma_V$  and to solve only for the turnover magnitude. Such an approach is expected to work essentially because, for giant ellipticals, the GCLF dispersion in its Gaussian form is observed to be highly consistent from one galaxy to another. For 13 gE galaxies with well measured GCLFs, Whitmore (1996) and Harris (1999) find  $\sigma_V = 1.4$  with an uncertainty of just  $\pm 0.05$ . In particular, this dispersion value fits the very thoroughly studied Virgo giant M87 quite well (see Harris et al. 1998b; Kundu et al. 1999). A further application of Blakeslee & Tonry’s (1995) variant of the SBF method to the GCLF may permit the removal of this constraint on  $\sigma_V$ .

For an initial fit, we use a Gaussian function and employ a  $\chi^2$  minimization to the binned data (second panel of Fig. 3). Table 4 summarizes the variety of parametric fits we obtained under the constraints listed. Employing the entire data range, i.e. includ-

TABLE 2  
TRANSFORMATION TERMS FOR WFPC2 CCDs

	PC1	WF2	WF3	WF4
Geometric Factor	-0.0071	-0.0005	0	-0.0014
Gain Factor	0.7455	0.7542	0.7558	0.7279
Aperture Correction				
F606W	$-0.26 \pm 0.10$	$-0.28 \pm 0.05$		
F814W	$-0.25 \pm 0.07$	$-0.28 \pm 0.05$		

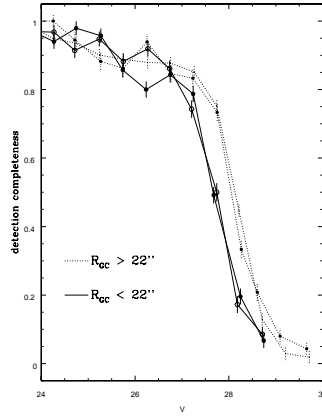


FIG. 2.— Detection efficiency as determined by artificial star tests. The inner rings (mostly drawn from the PC chip) displays brighter cutoffs, which are caused by the higher halo light level at small radii.



FIG. 3.— *Left panel:* The data defining the globular cluster luminosity function (GCLF). The open circles indicate the luminosity function of all starlike objects within  $75''$  of the galaxy center in 0.2-magnitude bins and corrected for incompleteness, while the open squares represent the LF at radii larger than  $75''$  with the counts normalized to the area of the inner region. *Right panel:* The points show the background-subtracted and completeness-corrected GCLF used for the  $\chi^2$  fits, now binned in 0.4-magnitude steps. The solid line is a Gaussian of width  $\sigma_V = 1.4$  and peak  $V^0 = 27.8$  (the “constrained” fit described in the text), while the dotted line is a Gaussian with  $\sigma_V = 1.49$  and peak  $V^0 = 28.0$  (the unconstrained maximum-likelihood fit). The short-dashed line indicates the 50% completeness level while the long-dashed line is the 5% completeness level.

TABLE 3  
LUMINOSITY FUNCTION DATA

$\langle m_V^0 \rangle$	Inner	$\pm$	Outer	$\pm$
23.2	3	2	0	0
23.3	1	1	2	1
23.5	5	2	1	1
23.7	2	1	2	1
23.9	9	3	3	2
24.1	4	2	1	1
24.3	18	4	7	3
24.5	22	5	10	3
24.7	31	6	17	4
24.9	38	6	23	5
25.1	49	7	16	4
25.3	71	9	34	6
25.5	76	9	55	9
25.7	92	10	40	7
25.9	107	11	41	7
26.1	129	12	57	8
26.3	166	14	60	9
26.5	160	13	93	11
26.7	191	15	100	12
26.9	228	16	109	12
27.1	262	18	147	14
27.3	261	17	160	16
27.5	273	18	120	12
27.7	301	21	127	14
27.9	255	21	125	15
28.1	252	25	66	12
28.3	253	28	100	17
28.5	235	34	59	17
28.7	153	36	32	14
28.9	98	37	24	17

TABLE 4  
GAUSSIAN REPRESENTATIONS OF THE GCLF

$m_V^0$	$\sigma_V$	$\chi^2$
$28.08 \pm 0.3$	$1.5 \pm 0.3$	1.4
$27.90 \pm 0.08$	1.4	1.4
$28.00^{+0.19}_{-0.22}$	$1.49 \pm 0.11$	ML <sup>b</sup>
$27.88 \pm 0.10$	1.4	ML <sup>c</sup>

<sup>a</sup>Values given without error ranges were constrained during fitting, error ranges given are  $1 \sigma_p$  uncertainties

<sup>b</sup>Maximum likelihood analysis

<sup>c</sup>Constrained maximum likelihood analysis

ing data even beyond the 50% completeness level, typically results in a best-fit Gaussian which is quite broad and whose peak is biased towards fainter magnitudes. This effect has been seen many times in the literature and is the result of the parametric correlation between  $V^0$  and  $\sigma_V$  mentioned above. The  $\chi^2$  fit is much more robust if only those objects brighter than the 50% completeness limit are used (see row one of the table) and the width is kept fixed at the canonical value of  $\sigma_V = 1.4$  (row two of the table). As seen in Table 4, this constrained fit results in a  $\chi^2$  which is little different from that of the unconstrained fit.

Next we employ a maximum-likelihood fit to the raw data following the precepts of Secker & Harris (1993). Here, the model Gaussian curve is convolved with the photometric completeness and photometric error functions and then matched to the raw, uncorrected GCLF. The results are shown in Table 4 and Figure 4.

An unconstrained fit for both  $V^0$  and  $\sigma_V$  (now excluding only those data fainter than the 5% completeness limit) again results in a fainter turnover and broader dispersion much as did the unconstrained  $\chi^2$  fit to the binned data. Also given in the table is the range of values of  $V^0$  consistent (at the  $1 \sigma$  level) with a Gaussian of width  $\sigma_V = 1.4$ . This range of values mimics that of the constrained  $\chi^2$  fit but make use of a larger magnitude range of the data.

The results of the unconstrained fits and those with  $\sigma_V$  set to 1.40 appear in the second panel of Figure 3. They are very similar. The history of GCLF

analysis can be a guide in our final choice of the turnover luminosity. For data which reach only to the turnover point or just past it, the unconstrained fits have almost always proven to yield overestimates of both the turnover and GCLF dispersion, with the benefit of hindsight and deeper data. We suggest that the most prudent choice is that of the constrained fits. There is little to choose between the maximum-likelihood and  $\chi^2$  approaches; we adopt  $V^0 = 27.88 \pm 0.12$  and  $\sigma_V = 1.49^{+0.15}_{-0.10}$  (fitting errors only), where the range of  $\sigma_V$  is that allowed via the maximum likelihood analysis.

Finally, we have followed exactly the analysis outlined above but this time using only the data from the inner region and without first subtracting a background. Fits to these “un-subtracted” data result in parameters identical to those we report here for the background subtracted  $\chi^2$  fits. The only difference found is in the allowed range of  $\sigma_V$  as reported via a maximum-likelihood analysis which reports an allowed range of  $1.7 < \sigma_V < 2.0$ . This extension of  $\sigma_V$  to larger values is the expected result if we assume that the majority of our background is derived from the mis-classification of faint background sources as stellar, thus elevating the faint-end of the luminosity function. By once again constraining the maximum-likelihood fits of the luminosity function of the inner region, requiring that  $\sigma_V = 1.40$ , we recover the results reported here for peak of the background subtracted distribution.

The Coma cluster is almost at the North Galactic Pole, with nearly negligible foreground extinc-

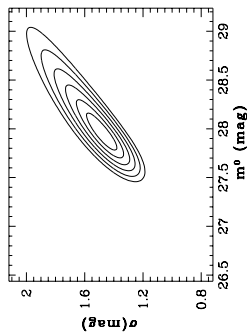


FIG. 4.— Maximum-likelihood contours (dispersion  $\sigma_V$  against turnover magnitude  $V^0$ ) for a Gaussian representation of the GCLF of NGC 4874. The most probable solution is  $\sigma_V = 1.49$ ,  $V^0 = 28.00$ ; the innermost contour is  $0.5 \sigma_p$  (standard deviations) with steps of  $0.5 \sigma_p$  between contours. Note that the two parameters are correlated, and the contours are asymmetric such that higher values of each are favored over lower ones.

tion. Here we adopt the same value as used by Baum et al. (1997) in their discussion of the GCLF in IC 4051, namely  $E(B-V) = 0.01$  and  $A_V = 0.03 \pm 0.01$ . We also include the minor  $K$  (cosmological redshift) correction of  $0.03 \pm 0.01$  as detailed in their analysis. Thus our turnover magnitude, dereddened and  $K$ -corrected, is  $V^0 = 27.88 - 0.06 \simeq 27.82 \pm 0.13$ .

Two other Coma ellipticals have GCLFs measured from deep HST photometry: NGC 4881 (Baum et al. 1995) and IC 4051 (Baum et al. 1997; Woodworth & Harris 1999). Both of these are normal, relatively isolated giant ellipticals on the outskirts of the cluster core. The NGC 4881 data do not reach faint enough to define the GCLF turnover unambiguously, and we will not use it here. However, the IC 4051 data are quite comparable in depth to our NGC 4874 measurements. For it, Baum et al. (1997) found  $V^0 = 27.79$  from the population of objects on only the PC1 frame<sup>3</sup>. Woodworth & Harris (1999), from an independent reduction of the same raw data but now including all four WFPC2 frames (thus doubling the globular cluster population compared with the PC1 alone) determined  $V^0 = 27.77 \pm 0.20$  (their quoted error includes the uncertainty of the fitted Gaussian parameters). We adopt for IC 4051 a mean value of  $V^0 = 27.72 \pm 0.20$  after the  $K$ -correction and extinction are subtracted.

The measured turnover levels of both galaxies – NGC 4874 and IC 4051 – agree at the 0.1-magnitude level, well within their combined uncertainty of  $\pm 0.25$  mag. A straight mean of the two gives  $V^0(\text{Coma}) = 27.77 \pm 0.10$ , which we use for the following discussion.

#### 4. CALIBRATING THE DISTANCE TO COMA

Once an intrinsic luminosity for  $M_V^0(\text{GCLF})$  is adopted, the distance to Coma follows immediately. In principle, we could take the value for  $M_V^0$  from the Milky Way GCLF and therefore jump from the Milky Way to Coma in a single step, bypassing the entire chain of distance indicators which leads through the Local Group, Virgo, Fornax, and so forth (e.g., Baum et al. 1997). However, the fundamental objection to such an approach is simply that we would be comparing two very different types of galaxies, in which it is possible that the globular cluster formation and evolution processes have been different. To avoid such concerns as much as possible and place our result on astrophysically more defensible ground, we choose instead to compare only giant ellipticals with giant ellipticals.

In essence then, to calibrate  $M_V^0$  we need to have well determined GCLFs in giant ellipticals (and preferably cD's as well) whose distances are themselves well established from more fundamental stellar standard candles. The largest nearby collections of such gE's are in the Virgo and Fornax clusters. Fortunately both of these have central cD-type galaxies (M87 in Virgo, NGC 1399 in Fornax) as well as many other giant ellipticals which provide highly effective tests of the empirical galaxy-to-galaxy scatter of the GCLF method (Whitmore 1996; Harris 1999).

Distance indicators applicable to these nearby galaxies are the red-giant-branch tip luminosity (TRGB), surface brightness fluctuations (SBF), planetary nebulae (PNLF), and of course Cepheid variables. These four methods have the strongest obser-

<sup>3</sup>We have adjusted their result to account for the 0.05 magnitude shift between long and short exposures as noted above; see e.g., Stetson et al. (1999).

vational claims to precisions approaching  $\pm 0.1$  mag, and their foundations are well understood from basic stellar physics (Jacoby et al. 1992; Lee et al. 1993; Ferrarese et al. 1999a). Results taken from the current literature are summarized in Tables 5 and 6.

Intercomparisons among these methods are still best done within the Virgo cluster, which has the richest variety of published results. For the seven published Virgo Cepheid galaxies, we reject only the result for NGC 4639 (which at  $(m-M)_0 = 31.8$  is  $\gtrsim 0.7$  mag more distant than the average of the other six, which are in close agreement; see the compilation of Ferrarese et al. 1999a. We also adopt the revised modulus for NGC 4535 as listed by Ferrarese et al. 1999b, containing the small correction for faint-end incompleteness.)

As can be seen in Table 5, there is remarkable consistency among the four methods, and we adopt a weighted-average true distance modulus of  $\mu_0(\text{Virgo}) = 30.99 \pm 0.03$ . We note that this mean would change to  $\simeq 31.01$  if we had adopted the  $\sim 0.1$ -mag larger SBF values listed by Ferrarese et al. (1999a). The quoted uncertainty represents the scatter among the individual methods and not the (much larger) external uncertainty in the fundamental distance scale calibration. These moduli are based on an adopted distance modulus  $\mu_0 = 18.5 \pm 0.1$  for the LMC, which provides the main underpinning for the Cepheid P-L relation. Thorough reviews of the basis for the LMC modulus, including re-assessments of the *Hipparcos* parallax data, are given by Carreta et al. (1999), Harris (1999), and Fernley et al. (1998) among others and need not be repeated here. In light of these discussions, we feel – perhaps optimistically – that the true external uncertainty in the Virgo distance is close to  $\pm 0.2$  mag.

The distance to Fornax is not as well determined: fewer galaxies have been studied; the differences among the PNLf, Cepheid and SBF distance estimates are larger than their internal error margins; and a TRGB calibration is not yet in hand. Of the three published Cepheid galaxies (again, with the incompleteness-corrected values from Ferrarese et al. 1999b), two (NGC 1326A, 1365) have published moduli  $\sim 0.2$  mag larger than the SBF or PNLf values, while the third (NGC 1425) is  $\sim 0.6$  mag larger. This discrepancy reinforces the serious concern that the outlying Cepheid spirals may either

be much more widely spread than the central ellipticals which are most relevant for GCLF studies, or at a different mean distance.<sup>4</sup>

In principle, a better way to approach the comparison is to use methods relating to the ellipticals alone. The measured GCLF turnovers of Virgo and Fornax E galaxies can be used to compute a relative Fornax-Virgo distance, with the *assumption* that they have fundamentally the same luminosity. Six ellipticals in each cluster have GCLFs measured to  $\gtrsim 1$  mag beyond the turnover point, with results as summarized in Table 7.

The difference between the weighted averages of  $V^0$  gives  $\Delta\mu(\text{Fornax-Virgo}) = 0.14 \pm 0.05$ . Adding this distance offset to the adopted Virgo modulus then suggests  $\mu_0(\text{Fornax, GCLF}) = 31.13 \pm 0.08$ . This value, in turn, is in entirely reasonable agreement with the SBF ( $31.23 \pm 0.06$ ) and PNLf ( $31.20 \pm 0.14$ ) determinations of the Fornax distance. However, it disagrees strongly with the mean Cepheid distance or with Ferrarese et al.’s recalibrated SBF value.<sup>5</sup> For the purposes of this discussion, we will defer further use of the Fornax system and employ only the Virgo ellipticals as our calibrators for the GCLF turnover luminosity.

There are two obvious ways to obtain the Coma/Virgo distance ratio through the GCLF data:

- (a) compare the GCLF turnovers of just the two central cD galaxies, M87 and NGC 4874; or
- (b) compare the mean GCLF turnovers of all Virgo giant ellipticals with the mean for our two Coma ellipticals.

The latter route has the advantage of greater statistical weight over many galaxies, while the former has the advantage of matching similar types of galaxies as strictly as possible, albeit at the cost of greater internal uncertainty. As we will see below, the two approaches turn out to agree quite well.

#### 4.1. M87 vs. NGC 4874

At various times in the literature, concerns have been raised regarding possible dependences of the GCLF shape and peak on environment, galaxy type, and cluster metallicity. By restricting the comparison to M87 and NGC 4874 alone, we can minimize these worries. Both are centrally placed giant ellipticals with cD envelopes, and though they are not

<sup>4</sup>Ferrarese et al. (1999a) adopt a recalibration of the SBF method which gives them a Fornax SBF modulus  $\sim 0.35$  mag larger than from Tonry et al. (1997), nominally bringing it into better agreement with the mean of the three Cepheid spirals. Considerable further work on the Fornax ellipticals through a variety of techniques is clearly called for to sort out these large uncertainties.

<sup>5</sup>Ferrarese et al. (1999a) conclude that the GCLF turnover luminosity is “a full 0.5 magnitude brighter” in Fornax than in Virgo. This conclusion is a direct result of their high adopted Fornax distance modulus  $(m-M)_0 \simeq 31.6$ . It should be emphasized that, although they use a less complete GCLF database than ours, their adopted mean *apparent* turnover magnitudes for both Virgo and Fornax are  $\lesssim 0.05$  mag different from our adopted means in Table 7 and thus not the source of the discrepancy. In our view, the best distance modulus to apply to the inner, GCLF-bearing *ellipticals* in Fornax is still very much less certain than for Virgo. Our contention is that the turnover luminosity difference between the Virgo and Fornax ellipticals is at the level of 0.2 mag or less (see the discussion below).

TABLE 5  
ESTIMATES OF DISTANCE TO VIRGO CLUSTER

Technique	$(m-M)_0$	Sources <sup>a</sup>
Cepheids	$31.02 \pm 0.04$	1,2,3,4,5,6
SBF	$31.02 \pm 0.05$	7,8,9,10
PNLF	$30.88 \pm 0.05$	11,12
TRGB	$30.98 \pm 0.18$	13
$\langle m-M \rangle_0$	$30.99 \pm 0.03$	

<sup>a</sup>Sources: (1) Ferrarese et al. 1996 (2) Pierce et al. 1994 (3) Saha et al. 1996a (4) Saha et al. 1996b (5) Graham et al. 1999 (6) Ferrarese et al. 1999b (7) Tonry et al. 1997 (8) Neilsen et al. 1997 (9) Pahre & Mould 1994 (10) Morris & Shanks 1998 (11) Jacoby et al. 1990 (12) Ciardullo et al. 1998 (13) Harris et al. 1998a

NOTE.—Uncertainties listed are the 1  $\sigma$  scatter among referenced sources, or the internal uncertainties quoted by the original authors.

TABLE 6  
ESTIMATES OF DISTANCE TO FORNAX CLUSTER

Technique	$(m-M)_0$	Sources <sup>a</sup>
Cepheids	$31.54 \pm 0.14$	1
SBF	$31.23 \pm 0.06$	2
PNLF	$31.20 \pm 0.07$	1,3
$\langle m-M \rangle_0$	$31.30 \pm 0.04$	

<sup>a</sup>Sources: (1) Ferrarese et al. 1999b (2) Tonry et al. 1997 (3) McMillan et al. 1993

TABLE 7  
GCLF TURNOVER MAGNITUDES FOR VIRGO AND FORNAX ELLIPTICALS

	Galaxy	$V^0(\text{turnover})$	Sources <sup>a</sup>
Virgo	N4472	$23.87 \pm 0.07$	1,2,3
	N4478	$23.82 \pm 0.38$	4
	N4486	$23.67 \pm 0.04$	5,6,7,8,9
	N4552	$23.70 \pm 0.30$	2
	N4649	$23.66 \pm 0.10$	1
	N4697	$23.50 \pm 0.20$	10
	Weighted Mean	$23.73 \pm 0.03$	
Fornax	N1344	$23.80 \pm 0.25$	11
	N1374	$23.52 \pm 0.14$	12
	N1379	$23.92 \pm 0.20$	12,13
	N1399	$23.86 \pm 0.06$	11,12,14,15
	N1404	$23.94 \pm 0.08$	11,15,16
	N1427	$23.78 \pm 0.21$	12
	Weighted Mean	$23.85 \pm 0.04$	

<sup>a</sup>Sources: (1) Secker & Harris 1993 (2) Ajhar et al. 1994 (3) Lee et al. 1998 (4) Neilsen et al. 1997 (5) Harris et al. 1991 (6) McLaughlin et al. 1994 (7) Whitmore et al. 1995 (8) Harris et al. 1998b (9) Kundu et al. 1999 (10) Kavalaars & Gladman 1998 (11) Blakeslee & Tonry 1996 (12) Kohle et al. 1996 (13) Elson et al. 1998 (14) Bridges et al. 1991 (15) Grillmair et al. 1999 (16) Richtler et al. 1992

identical in size or luminosity (NGC 4874 is a magnitude more luminous, and Coma is distinctly richer than Virgo), the comparison is certainly closer than with an average E galaxy. M87 has one of the best-studied of GCS luminosity functions: repeated observations to ever-increasing depth and radial coverage have extended the GCLF far past the turnover and have now made it possible (for example) to define GCLFs separately for the two parts of its clear bimodal color distribution or as a function of galactocentric distance.

For M87, the best determination of the GCLF turnover is by Kundu et al. (1999), who find  $V^0(\text{M87}) = 23.67 \pm 0.06$  from their deep WFPC2 photometry, after subtraction of an adopted foreground extinction  $A_V = 0.067 \pm 0.04$  mag. Subtracting  $V^0(\text{M87})$  from our NGC 4874 determination, we immediately derive  $\Delta\mu_0(\text{Coma-Virgo}) = 4.15 \pm 0.14$  (with the plausible assumption that both galaxies are at or near the physical centers of their clusters).

A further sophistication on this comparison can be taken if we look more narrowly at the metallicity and radial dependences. Several deep photometric studies (Grillmair et al. 1986; Lauer & Kormendy 1986; McLaughlin et al. 1994; Harris et al. 1998b; Kundu et al. 1999) show radial trends in the GCLF turnover can be ignored as the level of variation is at the  $\pm 0.2$ -mag level or less. For the metallicity issue, Whitmore et al. (1995) and Kundu et al. (1999) find that the peak of the M87 GCLF has a *small* – and perhaps not significant – dependence on color, where the GCLF may be  $\sim 0.1$  mag fainter for the redder, more metal-rich half of the bimodal color distribution. However, NGC 4874 differs from M87 in that its globular cluster color distribution is *not* bimodal: our two-color data indicate (Figure 5) that the mean color of the NGC 4874 GCS is very much like that of the bluer, more metal-poor half of the M87 cluster system. For the metal-poor component, Whitmore et al. find  $V^0(\text{M87, blue}) \simeq 23.6 \pm 0.1$  where the uncertainty includes both the photometric and fitting uncertainty combined as random errors.<sup>6</sup> In a new reduction of the same images, Kundu et al. find entirely similar results. If we then take  $V^0(\text{M87, blue}) = 23.6 \pm 0.1$  and subtract it from the NGC 4874 turnover, we obtain  $\Delta\mu_0(\text{Coma-Virgo}) = 4.22 \pm 0.16$ . However, it is not obvious that the metallicity offset is real or that it should be applied. Two counterarguments are the following:

(a) The Virgo and Fornax ellipticals display a wide variety of globular cluster color distributions – unimodal, bimodal, red, or blue (e.g., Neilsen & Tsve-

tanov 1999; Ajhar et al. 1994; Gebhardt & Kissler-Patig 1999; Kissler-Patig et al. 1997). These obvious differences in the metallicity distributions, however, do not result in any clearly correlated changes in the GCLF turnover points within a scatter of  $\pm 0.15$  mag (see below).

(b) The color distribution for the clusters in IC 4051, the other Coma giant, is entirely unimodal and *red*, just the opposite of NGC 4874 (Baum et al. 1997; Woodworth & Harris 1999). Yet its GCLF turnover differs from NGC 4874 by only 0.1 mag and is, if anything, *brighter*, contrary to the case for M87.

An alternate argument put forward by Blakeslee & Tonry (1996) is that the turnover of the GCLF depends on environment, represented by the velocity dispersion of the group of galaxies it is in. They suggest that the turnover becomes *less* luminous within *more* massive galaxy clusters (that is, ones with higher velocity dispersion); and if so, then we would be overestimating the true Coma turnover luminosity since it is a more massive environment than Virgo.

The empirical correlation for this effect is shown in Figure 6 (a replottting of Blakeslee & Tonry’s Figure 2, with the more recent values for  $M_V^0$  for a variety of GCLFs). The Leo data are taken from Kundu & Whitmore 1999, and M31, the Milky Way, and the Local Group dwarf ellipticals from the compilation of Harris 1999. Rather than mixing all types of parent galaxies, we restrict our attention to only the giant ellipticals (in the large disk galaxies and dE’s, the globular clusters may indeed have experienced very different tidal fields and thus degrees of dynamical destruction). We find a very much more modest trend than did Blakeslee & Tonry, well within the  $\sim 0.2$ -mag scatter expected from the data. Furthermore, it is not obvious just where along the horizontal axis of this graph Coma “belongs”, since there is abundant evidence (see Paper II for a summary) that it has assembled from a variety of smaller original clusters, structural traces of which are visible today in the galaxy spatial distributions and intracluster gas.

Our provisional conclusion is that, although *slight* dependences of GCLF turnover on such factors as metallicity, radius, and environment may be expected on current theoretical grounds, the weight of direct observational evidence indicates no such trends above the measurement scatter of the method. For the *present*, we therefore choose not to apply any such adjustments to the GCLFs until such time as they are considerably more well established on strict empirical grounds.

<sup>6</sup>Whitmore et al. do not state an uncertainty for their determination of  $V^0$ ; we take it to be their quoted fitting error for the entire GCLF, increased by  $\sqrt{2}$  to allow for the smaller sample size of the metal-poor cluster population relative to the total population.

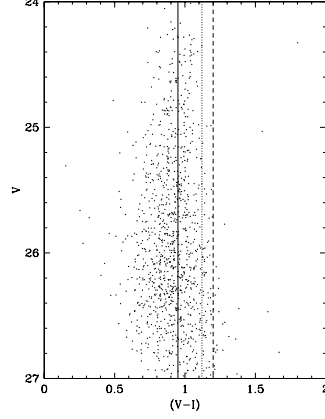


FIG. 5.—  $(V-I)$  colors of starlike objects within  $70''$  of the center of NGC 4874. Objects with photometric measurement uncertainties less than  $\epsilon(V-I) = 0.07$  are plotted. The mean color of the globular cluster population is  $\langle V-I \rangle \simeq 0.95$ , which is similar to the metal-poor cluster population of M87 (solid line). For comparison, the long dashed line is the mean color of the metal-rich component of the M87 GCS and the dotted line is the mean  $(V-I)$  of the entire M87 GCS (Whitmore et al. 1995; Kundu et al. 1999).

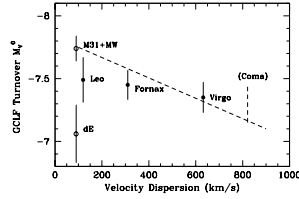


FIG. 6.— GCLF turnover luminosity  $M_V^0$  plotted against the velocity dispersion of the host cluster of galaxies. *Filled symbols* represent the giant E galaxies in Leo, Fornax, and Virgo, from the most recent determinations of their distances and GCLF observations. *Open symbols* show the disk and dwarf E members of the Local Group. The location of the two Coma galaxies is shown by the vertical dashed line at right, while the proposed correlation from Blakeslee & Tonry (1996) is shown as the long dashed line. See text for discussion.

#### 4.2. The Virgo Ellipticals vs. the Coma Ellipticals

Our second approach is simply to take the average turnover luminosity of all the ellipticals in both clusters. In doing so, we deliberately average over (or in effect, ignore) any differences in metallicity, elliptical type, or sample differences in radial location. It is *empirically* true that all these effects are minor: for a sample of 17 giant ellipticals with well measured GCLFs and fundamental distance calibrations (Virgo, Fornax, and a handful of others at similar distances), the turnover luminosity exhibits a galaxy-to-galaxy scatter of  $\pm 0.15$  mag (Harris 1999; Whitmore 1996). For six Virgo gE's including M87, Table 7 shows  $V^0 = 23.71 \pm 0.03$ , a number which is indistinguishable from our adopted value for the M87 peak by itself though it is internally more precise. Thus, by this approach we obtain  $\Delta\mu(\text{Coma-Virgo}) = (28.77 \pm 0.10) - (23.71 \pm 0.03) = 4.06 \pm 0.11$ .

All the results derived here for the relative Coma/Virgo modulus agree with each other within their internal uncertainties, and there is no evidence that any of the factors mentioned above (cD vs. normal giant elliptical; cluster metallicity; radial location) produce measurable systematic biases to within the  $\pm 0.1$ -mag fitting uncertainties built into the GCLF method. We therefore adopt the last of the determinations listed above ( $\Delta\mu = 4.06 \pm 0.11$ ), which has the highest internal precision and greatest statistical security of sample size. Adding this to our adopted Virgo distance modulus, we obtain  $\mu(\text{Coma}) = 35.05 \pm 0.12$  or  $d = (102 \pm 6)$  Mpc (where the quoted error represents only the internal uncertainty of the method).

Earlier literature (see, e.g., Capaccioli et al. 1990; Sandage & Tammann 1990; van den Bergh 1992 for reviews of a range of methods) tended to give  $\Delta\mu(\text{Coma} - \text{Virgo})$  in the range 3.7–3.8. However, our determination of 4.06 is similar to other, more recent determinations that rely directly on the giant ellipticals: for example, SBF analysis of ellipticals in Coma and Leo I (Thomsen et al. 1997) and the fundamental plane comparison for the Leo and Coma ellipticals (Hjorth & Tanvir 1997) give  $\Delta\mu(\text{Coma} - \text{Leo}) \simeq 4.8 - 4.9$ . Subtracting  $\Delta\mu(\text{Virgo} - \text{Leo}) = 0.87 \pm 0.1$  (Ferrarese et al. 1999a) then gives  $\Delta\mu \simeq 4.0$  to 4.1 for the Virgo-to-Coma step, in agreement with our findings.

The GCLF turnover luminosity that we implicitly adopt along with this distance calibration is, *from the Virgo cluster alone*,  $M_V^0 = -7.26 \pm 0.06$  (internal uncertainty). For Fornax alone, our turnover luminosity would be  $M_V^0 = -7.45 \pm 0.06$ . The true external uncertainties on both of these estimates, particularly for

Fornax, are likely to be near  $\pm 0.2$  mag.

#### 5. THE HUBBLE CONSTANT

We can now estimate  $H_0$ . The redshift of Coma corrected for Local Group peculiar motion (e.g., Colless & Dunn 1996) is  $cz = 7100 \text{ km s}^{-1}$ , with a likely uncertainty of  $\pm 200 \text{ km s}^{-1}$  taking into account the degree to which the peculiar velocities of the Milky Way and Local Supercluster relative to the CMB are known. We note that this mean Coma velocity explicitly excludes the outlying NGC 4839 subgroup, which would have biased the mean to slightly higher levels (see Colless & Dunn 1996).

From Hubble's law,  $cz = H_0 \cdot d$ , we obtain

$$H_0 = cz \cdot 10^{(5-0.2\mu_0)} \text{ km s}^{-1} \text{ Mpc}^{-1}.$$

Corrections for the geometric curvature parameter  $q_0$  are negligible (if  $q_0$  is in the range  $\sim 0.0 - 0.5$ , at the Coma redshift of  $z = 0.0237$  the resulting uncertainty in  $H_0$  is only 0.3 percent). Putting in our distance modulus and redshift for Coma, we obtain  $H_0 = 69 \text{ km s}^{-1} \text{ Mpc}^{-1}$ .

The net uncertainty in our result must include not only the internal uncertainties of the Coma/Virgo relative distance and the CMB-corrected Coma velocity, but also a series of other external uncertainties. The true (external) error is dominated by the uncertainty in the fundamental distance scale that enters our discussion through the Virgo distance. This calibration depends in turn on a multitude of connected issues such as the distance to the LMC and the parallaxes of nearby standard candles (RR Lyraes, Cepheids, subdwarfs). A full discussion of these issues is far beyond the scope of this paper, but our reading of the literature suggests that the external uncertainty in the Virgo distance modulus may now be at the level of  $\pm 0.2$  mag.

Table 8 contains a complete review of our error budget. Combining the uncertainties in quadrature, and without distinguishing them rather arbitrarily as “internal” or “external”, we derive for our final estimate

$$H_0 = (69 \pm 9) \text{ km s}^{-1} \text{ Mpc}^{-1}.$$

The Coma galaxies are easily the most remote ones for which GCLF turnover levels have been directly measured, and thus they exert the most leverage on any estimates of  $H_0$  with this technique. However, as a last useful check on the result, we can display the GCLF results for several galaxies and clusters in a classic “Hubble diagram”: that is, a plot of redshift against the apparent magnitude of the turnover.

TABLE 8  
ERROR BUDGET FOR OUR  $H_0$  MEASUREMENT

...	uncertainty source	km s <sup>-1</sup> Mpc <sup>-1</sup>
$\pm 0.25 \Delta q_0$	curvature parameter $q_0$ :	$\pm 0.2$
$\pm 0.04$ mag	foreground extinction:	$\pm 1.3$
$\pm 0.05$ mag	WFPC2 photometric zeropoint:	$\pm 1.6$
$\pm 200$ km s <sup>-1</sup>	Coma CMB-corrected redshift:	$\pm 2.0$
$\pm 0.1$ mag	turnover luminosity (blue vs. red):	$\pm 3.3$
$\pm 0.11$ mag	GCLF turnovers (Coma <i>minus</i> Virgo):	$\pm 3.6$
$\pm 0.2$ mag	Virgo distance modulus:	$\pm 6.8$

Hubble's law can be rewritten as

$$\log cz = 0.2V^0 + \log H_0 - 0.2M_V^0 - 5$$

where  $M_V^0$  is the GCLF turnover luminosity for giant E galaxies, and  $H_0$  is expressed in its usual units.

Relevant data for a total of 10 galaxies or groups are listed in Table 9 and plotted in Figure 7

(See Harris 1999 for the first use of this Hubble diagram for GCLFs). In this table, the entries for Virgo and Fornax are the weighted mean  $\langle V^0 \rangle$  values listed previously, while the entry for the nearby Leo I system is the average of NGC 3377 and 3379 from Kundu & Whitmore 1999. The cosmological recession velocities ( $cz$ ) assume a Local Group infall to Virgo of  $250 \pm 100$  km s<sup>-1</sup> (e.g., Ford et al. 1996; Hamuy et al. 1996; Jerjen & Tammann 1993, among others). The mean radial velocities of each galaxy or group are taken from Faber et al. (1989), Girardi et al. (1993), Huchra (1988), Binggeli et al. (1993), Hamuy et al. (1996), and Colless & Dunn (1996).

The last four entries in Table 9 are from Lauer et al. 1998 for brightest cluster ellipticals (BCG's) in four Abell clusters. These authors assume a Gaussian GCLF shape with  $\sigma_V = 1.4$  (strictly comparable with what we use here), and then derive the  $V^0$  which best fits the measured luminosity function.

The solid line in Figure 7 is the solution for  $H_0 = 70$  and  $M_V^0 = -7.3$  (the mean luminosity of the GCLF turnover with our adopted Virgo calibration). The raw scatter of the points around the line is  $\pm 0.25$  mag rms, an independent estimate of the accuracy of the GCLF technique that is encouragingly similar to our global error budget summed above. Interestingly, the four nearest points (Leo I, Virgo, Fornax, and NGC 5846) are all on the high side of the line; with our adopted  $cz$  values as they stand, these four points by themselves would give  $H_0 \simeq 78$ . Conversely, they would all lie precisely on the mean line for  $H_0 = 70$

if their CMB-frame redshifts were reduced by 200 km s<sup>-1</sup> from the values listed in Table 9. The dashed lines in Figure 7 show the range that points would be expected to fall within purely by random velocity errors of  $\pm 200$  km s<sup>-1</sup>. The importance of obtaining galaxies at the largest possible distances to circumvent systematic errors on  $H_0$  is evident.

## 6. SUMMARY

1. Using the Hubble Space Telescope WFPC2 we have obtained deep images of the GCS of NGC 4874, the central cD in COMA. Photometry with DAOPHOT/ALLFRAME provides us with a measurement of the globular cluster luminosity function which reaches a 50% completeness at apparent magnitude  $V = 28.2$ .
2. Using both a constrained  $\chi^2$  and maximum likelihood analysis we find that the best-fit Gaussian for the GCLF of NGC 4874 has a turnover at  $V^0 = 27.82 \pm 0.13$  for a Gaussian of width  $\sigma_V = 1.4$ , and corrected for foreground absorption and  $K$ -correction. Combining this measurement with previous determinations of the GCLF turnover for another Coma elliptical, IC 4051, yields an average turnover value of  $V^0 = 27.77 \pm 0.10$  for Coma.
3. Comparing the Coma turnover value with the average value for six well studied ellipticals in Virgo implies a relative Coma/Virgo distance modulus  $\Delta\mu_0 = 4.06 \pm 0.11$ . Adding the Virgo distance as calibrated from the mean of the SBF, PNLf, TRGB and Cepheid techniques results in an intrinsic Coma distance modulus of  $\mu_0 = 35.05 \pm 0.13$  (internal error).
4. Adopting a recession velocity of  $v_r = 7100 \pm 200$  km s<sup>-1</sup> for Coma yields a Hubble constant

TABLE 9  
GCLF TURNOVER LEVELS IN DISTANT ELLIPTICALS

Cluster	Galaxy	Redshift $cz$	$V^0(\text{GCLF})$	Sources <sup>a</sup>
Leo I	2 gE's	850 km s <sup>-1</sup>	$22.61 \pm 0.33$	1
Virgo	6 gE's	1300	$23.71 \pm 0.03$	2
Fornax	6 gE's	1400	$23.85 \pm 0.04$	2
NGC 5846	NGC 5846	2300	$25.08 \pm 0.10$	3
Coma	IC 4051	7100	$27.75 \pm 0.20$	4
Coma	NGC 4874	7100	$27.82 \pm 0.12$	2
A 262	NGC 705	4650	$26.95 \pm 0.3$	5
A 3560	NGC 5193	4020	$26.12 \pm 0.3$	5
A 3565	IC 4296	4110	$26.82 \pm 0.3$	5
A 3742	NGC 7014	4680	$26.87 \pm 0.3$	5

<sup>a</sup>Sources: (1) Harris 1990 (2) This paper (3) Forbes et al. 1996a  
(4) Woodworth & Harris 1999 (5) Lauer et al. 1998

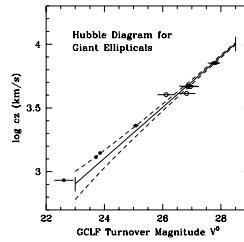


FIG. 7.— Hubble diagram for the GCLF technique. Here, galaxy redshift  $cz$  (km s<sup>-1</sup>) is plotted against the apparent magnitude  $V^0$  of the GCLF turnover (corrected for foreground extinction  $A_V$ ). Data points are taken from Table 9. The solid line has a slope 0.2 (see Section 5 of the text) and a zeropoint corresponding to  $H_0 = 70$  and  $M_V^0 = -7.3$ . Vertical tick marks at either end of the line show the range  $\Delta H_0 = \pm 9$  allowed by our determination. Filled circles are the galaxies with direct GCLF observations past the turnover point, while open circles are the four galaxies with deduced  $V^0$  values from SBF analysis. The *dashed lines* show the expected range within which points would fall if the redshifts  $cz$  are uncertain by  $\pm 200$  km s<sup>-1</sup>; see text.

of  $H_0 = 69 \text{ km s}^{-1} \text{ Mpc}^{-1}$ . A full error budget suggests that the true uncertainty in this estimate is  $\pm 9 \text{ km s}^{-1} \text{ Mpc}^{-1}$  or 13%; the dominant term is the uncertainty in the distance to Virgo, which we use as our fundamental calibrating point for GCLFs in giant ellipticals.

Further improvements in the range of allowed values for  $H_0$  will come with (a) the addition of more galaxies in Coma and other distant clusters, (b) con-

tinued effort to determine the true dependence of the GCLF peak on metallicity, and (c) more certain calibrations of the distances to the LMC, Fornax, Virgo, as the most fundamental stepping stones in the distance ladder.

This research was supported through grants from the Natural Sciences and Engineering Research Council of Canada.

## REFERENCES

- Ajhar, E. A., Blakeslee, J. P., & Tonry, J. L. 1994, *AJ*, 108, 2087  
 Ashman, K. M., Conti, A., & Zepf, S. E. 1995, *AJ*, 110, 1164  
 Baum, W. A. et al. 1995, *AJ*, 110, 2537  
 Baum, W. A. et al. 1997, *AJ*, 113, 1483  
 Binggeli, B., Popescu, C. C., & Tammann, G. A. 1993, *AApS*, 98, 275  
 Blakeslee, J. P., & Tonry, J. L. 1995, *ApJ*, 442, 579  
 Blakeslee, J. P., & Tonry, J. L. 1996, *ApJ*, 465, L19  
 Bridges, T. J., Hanes, D. A., & Harris, W. E. 1991, *AJ*, 101, 469  
 Capaccioli, M., Cappellaro, E., Della Valle, M., D'Onofrio, M., Rosino, L., & Turatto, M. 1990, *ApJ*, 350, 110  
 Carretta, E., Gratton, R. G., Clementini, G., & Fusi Pecci, F. 1999, preprint (astro-ph/9902086)  
 Ciardullo, R., Jacoby, G. H., Feldmeier, J. J., & Bartlett, R. E. 1998, *ApJ*, 492, 62  
 Colless, M., & Dunn, A. M. 1996, *ApJ*, 458, 435  
 Elson, R. A. W., Grillmair, C. J., Forbes, D. A., Rabban, M., Williger, G. M., & Brodie, J. P. 1998, *MNRAS*, 295, 240  
 Faber, S. M. et al. 1989, *ApJS*, 69, 763  
 Fernley, J. et al. 1998, *AAp*, 330, 515  
 Ferrarese, L. et al. 1996, *ApJ*, 464, 568  
 Ferrarese, L. et al. 1999, *ApJ*, in press (astro-ph/9908192)  
 Ferrarese, L. et al. 1999, *ApJS*, in press (astro-ph/9910501)  
 Forbes, D. A. 1996, *AJ*, 112, 954  
 Ford, H. C., Hui, X., Ciardullo, R., Jacoby, G. H., & Freeman, K. C. 1996, *ApJ*, 458, 455  
 Gebhardt, K., & Kissler-Patig, M. 1999, *AJ*, 118, 1526  
 Girardi, M., Biviano, A., Giuricin, G., Mardirossian, F., & Mezzetti, M. 1993, *ApJ*, 404, 38  
 Graham, J. A. et al. 1999, *ApJ*, 516, 626  
 Grillmair, C. J., Pritchet, C. J., & van den Bergh, S. 1986, *AJ*, 91, 1328  
 Grillmair, C. J., Forbes, D. A., Brodie, J. P., & Elson, R. A. W. 1999, *AJ*, 117, 167  
 Hamuy, M., Phillips, M. M., Suntzeff, N. B., Schommer, R. A., Maza, J., & Avilés, R. 1996, *AJ*, 112, 2398  
 Hanes, D. A., & Whittaker, D. G. 1987, *AJ*, 94, 906  
 Harris, W. E. 1987, *ApJ*, 315, L29  
 Harris, W. E. 1990, *PASP*, 102, 966  
 Harris, W. E. 1999, Lectures for 1998 Saas-Fee Advanced School on Star Clusters, in press  
 Harris, W. E., Allwright, J. W. B., Pritchet, C. J., & van den Bergh, S. 1991, *ApJS*, 76, 115  
 Harris, W. E., Durrell, P. R., Pierce, M. J., & Secker, J. 1998a, *Nature*, 395, 45  
 Harris, W. E., Harris, G. L. H., & McLaughlin, D. E. 1998b, *AJ*, 115, 1801  
 Harris, W. E., Kavelaars, J. J., Hanes, D. A., Hesser, J. E., & Pritchet, C. J. 1999, *ApJ*, in press  
 Hjorth, J., & Tanvir, N. R. 1997, *ApJ*, 482, 68  
 Holtzman, J. et al. 1995, *PASP*, 107, 1065  
 Huchra, J. P. 1988, in *The Extragalactic Distance Scale*, ASP Conf. Series 4, ed. S. van den Bergh & C. J. Pritchet (San Francisco: ASP), 257  
 Jacoby, G. H., Ciardullo, R., & Ford, H. C. 1990, *ApJ*, 356, 332  
 Jacoby, G. H. et al. 1992, *PASP*, 104, 599  
 Jerjen, H., & Tammann, G. A. 1993, *AAp*, 276, 1  
 Kavelaars, J. J., & Gladman, B. 1998, in *Proc. 5th CFHT Users Meeting*, ed. P. Martin & S. Rucinski (Kamuela: CFHT), 155  
 Kissler-Patig, M., Kohle, S., Hilker, M., Richtler, T., Infante, L., & Quintana, H. 1997, *AAp*, 319, 470  
 Kohle, S., Kissler-Patig, M., Hilker, M., Richtler, T., Infante, L., & Quintana, H. 1996, *AAp*, 309, L39  
 Kron, R. 1980, *ApJS*, 43, 305  
 Kundu, A., & Whitmore, B. C. 1999, *Bull. AAS*, 31, 874  
 Kundu, A., Whitmore, B. C., Sparks, W. B., Macchetto, F. D., Zepf, S. E., & Ashman, K. M. 1999, *ApJ*, 513, 733  
 Lauer, T. R., & Kormendy, J. 1986, *ApJ*, 303, L1  
 Lauer, T. R., Tonry, J. R., Postman, M., Ajhar, E. A., & Holtzman, J. A. 1998, *ApJ*, 499, 577  
 Lee, M. G., Freedman, W. L., & Madore, B. F. 1993, *ApJ*, 417, 553  
 Lee, M. G., Kim, E., & Geisler, D. 1998, *AJ*, 115, 947  
 Madore, B. F. et al. 1999, *ApJ*, 515, 29  
 McLaughlin, D. E., Harris, W. E., & Hanes, D. A. 1994, *ApJ*, 422, 486  
 McMillan, R., Ciardullo, R., & Jacoby, G. H. 1993, *ApJ*, 416, 62  
 Morris, P. W., & Shanks, T. 1998, *MNRAS*, 298, 451  
 Neilsen, E. H. Jr., & Tsvetanov, Z. I. 1999, *ApJ*, 515, L13  
 Neilsen, E. H. Jr., Tsvetanov, Z. I., & Ford, H. C. 1997, *ApJ*, 483, 745  
 Pahre, M. A., & Mould, J. R. 1994, *ApJ*, 433, 567  
 Pierce, M. J., Welch, D. L., McClure, R. D., van den Bergh, S., Racine, R., & Stetson, P. B. 1994, *Nature*, 371, 385  
 Richtler, T., Grebel, E. K., Domgorgen, H., Hilker, M., & Kissler, M. 1992, *AAp*, 264, 25  
 Saha, A., Sandage, A., Labhardt, L., Tammann, G. A., Macchetto, F. D., & Panagia, N. 1996a, *ApJ*, 466, 55  
 Saha, A., Sandage, A., Labhardt, L., Tammann, G. A., Macchetto, F. D., & Panagia, N. 1996b, *ApJS*, 107, 693  
 Sandage, A., & Tammann, G. A. 1990, *ApJ*, 365, 1  
 Secker, J., & Harris, W. E. 1993, *AJ*, 105, 1358  
 Stetson, P. B. 1987, *PASP*, 99, 191  
 Stetson, P. B. 1994, *PASP*, 106, 250  
 Stetson, P. B. et al. 1999, *AJ*, 117, 247  
 Thompson, L. A., & Valdes, F. 1987, *ApJ*, 315, L35  
 Thomsen, B., Baum, W. A., Hammergren, M., & Worthey, G. 1997, *ApJ*, 483, L37  
 Tonry, J. L., Blakeslee, J. P., Ajhar, E. A., & Dressler, A. 1997, *ApJ*, 475, 399  
 van den Bergh, S. 1992, *PASP*, 104, 861  
 Whitmore, B. C. 1996, in *The Extragalactic Distance Scale*, ed. M. Livio, M. Donahue, & N. Panagia (Baltimore: StScI), 254  
 Whitmore, B. C., Sparks, W. B., Lucas, R. A., Macchetto, F. D., & Biretta, J. A. 1995, *ApJ*, 454, L73  
 Woodworth, S., & Harris, W. E. 1999, in preparation